TRANSIENT CHARACTERISTICS OF DENSE GAS DISPERSION AS DEPICTED BY A DEPTH AVERAGED NUMERICAL MODEL

by

R. N. Meroney*

Prepared for Submission to

JOURNAL OF HAZARDOUS MATERIALS

Fluid Mechanics and Wind Engineering Program
Department of Civil Engineering
Colorado State University
Fort Collins, CO 80523

* Professor, Civil Engineering

CEP83-84RNM7

TRANSIENT CHARACTERISTICS OF DENSE GAS DISPERSION AS DEPICTED BY A DEPTH AVERAGED NUMERICAL MODEL

by

Robert N. Meroney

SUMMARY:

A depth integrated numerical model is used to calculate the behavior of heavy and cold gas clouds. The cold cloud may be heated from below or entrain moist air, and the entrainment velocities are influenced by cloud stratification. Experimental data on heavy gas dispersion are predicted accurately. The model reveals the characteristics of upwind motion of the gases at the source, gravity waves induced on the cloud top by wind shear, and the variable hazard zones associated with gases released instantaneously, over a finite time and continuously.

INTRODUCTION:

The use and transport of combustible hydrocarbon fuels having boiling points below ambient temperatures (liquefied natural gas (LNG), ethane, propane or butane (LPG)) or similar storage and handling of toxic gases (ammonia, chlorine, sulfur dioxide, of hydrogen sulfide) invites questions concerning the consequences resulting from accidental release. Often such gases have molecular or temperature characteristics which result in negatively buoyant gas clouds which hug the ground and extend the hazard zone in time and space. This paper uses a depth integrated numerical model to illuminate the fluid physics of dense plumes during period of gravity spread/air entrainment dominance.

A collection of papers which summarize field and laboratory measurements as well as the performance of several numerical models for dense gases was recently published by Britter and Griffiths (1982). Subsequently Meroney and Lohmeyer (1982, 1983a) and Meroney (1983) described further laboratory measurements for sudden releases of dense

gas volumes. Models proposed to predict the behavior of dense gas dispersion fall into five categories of increasing sophistication and plume physics:

a) Modifications of classical gaussian plume formulae developed for passive gases,

b) Gravitational spread models which establish plume shape prior to a passive diffusion phase,

c) Volume integrated box models,

d) Depth averaged slab models, and

e) Direct solution of the full three dimensional conservation equations by finite difference or finite element approaches.

Most models are distinguished from one another by the various ad hoc assumptions used for the mixing rates and duration chosen for the gravity spread phase. Since various constants must be specified from experimental data the results are often dependent on the data set used to calibrate the calculation scheme. Systematic calculations with the physically realistic slab or primitive equation models provide an opportunity to examine transient plume characteristics often seen in the field but difficult to measure accurately. This paper will use a computationally fast slab model to examine the following dense gas cloud characteristics:

a) Character of the upwind motion and breaking of the head wave,

b) Evidence for gravity waves on the cloud upper surface,

c) Source behavior during instantaneous, finite time, and continuous gas release, and

d) Shape of transient ignition zones.

The following sections describe the formulation of a depth average model, its credibility based on comparison to some field experiments, and numerical experiments to respond to the points raised above.

FORMULATION OF LAYER AVERAGED EQUATIONS:

A model for dense cloud dispersion is desired which reproduces the detailed nuances of behavior perceived during laboratory and field experiments. Three-dimensional calculations are very expensive of computer storage and time. Fortunately, when the flow situation is only weakly three dimensional, so that one dimension can be decoupled from the other two, a set of relations obtained by integrating the conservation equations over that dimension realistically describes fluid motions. To be accurate the "depth averaged" equations must have negligible vertical or lateral dynamic pressure gradients. Flow quantitites are generally assumed to be constant or have a similar distribution in the vertical and lateral directions.

The layer averaged (slab) model described below solves the depth averaged lateral and longitudinal momentum, mass continuity, concentration and enthalpy equations for longitudinally varying depth and width and cross section averaged densities, temperatures, velocities, and concentrations. The model does not make the Boussinesq assumption (i. e. vertical velocities are assumed to be small). Model constants are tuned to fit the data of Meroney and Lohmeyer (1982) or Andreiev, Neff and Meroney (1983).

Layer Averaged Equations:

The layer averaged equations can be written for two dimensional, radially symmetric, or laterally symmetric geometries. Two dimensional and radially symmetric geometries are discussed by Meroney and Lohmeyer (1983); hence a laterally symmetric form of the equations will be provided here. The layer-averaged value of a mean variable ϕ is defined as

$$\phi = 1/H \int_o^H \int_o^B \phi(x,y,z)\, dydz$$

Since mean variables are assumed distributed in a similar manner over the cross section covariances $\overline{\phi_a \phi_b}$ can be approximated as $\overline{\phi_a \phi_b} = \overline{\phi_a} \cdot \overline{\phi_b}$, and any errors are considered effective stresses and are included in diffusion terms. When entrainment takes place across H, where H is the upper boundary of the cloud, then the upper boundary must obey

$$\frac{dH}{dt} + U_T \frac{dh}{dx} = W_T + w_e,$$

where U_T and W_T are the mean horizontal and vertical velocities at H and w_e is the entrainment rate across H. The mean hydrostatic pressure within the layer is found from

$$(p(x) - p_a(H)) = \frac{g}{H} \int_o^H \int_o^{z'} (\rho - \rho_a)\, dz'dz$$

With the aid of the Leibnitz rule the conservation equations can be integrated over the cross section areas. The final equations developed were nondimensionalized with respect to time and space scales equal to $T = H_o^{1/2}(g_o')^{-1/2}$ and $L = H_o$ respectively where $g_o' = g(SG_o - 1)$. The final expressions used are:

Width Equation:

$$\frac{dB}{dt} + U\frac{dB}{dx} = 2(V_g + v_e), \tag{1}$$

Lateral Momentum Equation:

$$\frac{dM}{dt} + \frac{dUM}{dx} = \beta_1 - \frac{(R-1)}{(R_o-1)} H^2 - \frac{Cf}{2} RV_g^2(B_w - B_o)(HS) \tag{2}$$

$$+ \frac{1}{Re_T} \frac{d}{dx} \left(\frac{d(M)}{dx}\right)$$

Mass Conservation Equation:

$$\frac{dN}{dt} + \frac{dUN}{dx} = w_e B + 2v_e H + RW_o B_o \tag{3}$$

$$+ \frac{1}{Re_T} \frac{d}{dx} \left(\frac{d(N)}{dx}\right)$$

Mass Fraction Conservation Equation:

$$\frac{dP}{dt} + \frac{dUP}{dx} = R_o W_o B_o + \frac{1}{Re_T} \frac{d}{dx} \left(\frac{d(P)}{dx}\right) \tag{4}$$

Longitudinal Momentum Equation:

$$\frac{dK}{dt} + \frac{dUK}{dx} = -\frac{\beta_1}{2} \frac{d}{dx} \left(\frac{H^2 B(R-1)}{(R_o-1)}\right) \tag{5}$$

$$- \frac{Cf}{2} RU^2(B - B_o)(HS)$$

$$+U_a(w_e B + 2v_e H) + \frac{1}{Re_T} \frac{d}{dx} \left(\frac{d(K)}{dx}\right)$$

Enthalpy Conservation Equation:

$$\frac{dQ}{dt} + \frac{dUQ}{dx} = R_o E_o W_o B_o + E_a(w_e B + 2v_e H) \tag{6}$$

$$+ h_s T(B - B_o)(HS) + \frac{1}{Re_T} \frac{d}{dx} \left(\frac{d(Q)}{dx} \right)$$

$$+ (HS)(L_h)(\omega_{\phi, T_a} - \omega_{100, T}) \cdot$$

$$(w_e B + 2v_e H - R_o W_o B_o)$$

$$+ (HS)(L_h) RB(1 - C) \omega_{100, T} \frac{4886.}{T^2} (T_a - T_o) \frac{dT}{dx}$$

where

$M = RV_g HB$ $\qquad$ $N = RHB$

$P = RCHB$ $\qquad$ $K = RUHB$

$Q = REHB$

$R = 1/((1 - \theta T)(1-C+C(1-\beta))$

$E = -(1+Cs_m)T/(1+s_m)$

$X = C(1-\beta)/(1-C+C(1-\beta))$

$L_h = (\ell_{H_2O})/(c_{po}(T_a - T_o)$

$$h_s = \left(\frac{Gr}{Re^3 Pr} Ri^* \right)^{1/2} \frac{(1+Cs_m)}{(1+s_m)} RT^{1/2}$$

$$Gr = \frac{g\beta(T_a - T_o)H_o}{\nu_a^2}$$

$$Re = \frac{(g_o' H)^{1/2} H}{\nu_a} \quad , \quad \frac{1}{Re_T} = \text{Small numerical diffusivity to maintain stability}$$

$$Ri_* = \frac{(g_o')H_o}{u_*^2}$$

$$U_a = \frac{1}{k} Ri_*^{1/2} \ln(H/z_o + 1)$$

$$\beta = 1 - \frac{M_a}{M_o}$$

$$\theta = 1 - \frac{T_o}{T_a}$$

$$s_m^* = \frac{c_{po}}{c_{pa}} - 1$$

Heat Transfer Relations:

The above relations include the effects of gas mixture on properties, and the influence of humidity during condensation and re-evaporation is included in the enthalpy conservation equation. The dimensionless heat transfer coefficient is based on the bulk transfer coefficient for mixed free and forced convection in the atmosphere recommended by Leovy (1969). (HS) is the Heavyside operator for $T \gtrless T_{dewpoint}$.

Entrainment Model:

Entrainment rates are perturbations on the forms suggested by Eidsvik (1980) and Ermak et al. (1982), and other forms tried are reviewed in Meroney and Lohmeyer (1982). The entrainment expressions are:

$$w_e = c_z V_g + \frac{\alpha_4 \, v_*}{\frac{\alpha_4}{\alpha_6} + \frac{Ri_*}{RH^2}}$$

$$v_e = \frac{3.24 H v_*}{B}$$

$$v_*^2 = \alpha_3^2 / Ri_* + \frac{\alpha^2 \, Gr \, (1 + s_m)(1 - \theta T)}{Re^2 (1 + C s_m)(1 - \theta)} \, Hh_s T^{2/3}$$

Numerical Scheme:

Constants found to fit the wind-tunnel data most satisfactorily are $c_z = 0.05$, $\alpha_2 = 0.5$, $\alpha_3 = 1.0$, $\alpha_4 = 2.0$, $\alpha_6 = 0.3$, $\beta_1 = 0.153$, and $\alpha_7 = 3.5$. Equations (1) to (6) were developed in a difference form using an implicit, second-upwind-difference, donor-cell approach. The difference equations were solved by the Thomas algorithm. Step sizes in time were limited to:

$$\Delta t < \frac{0.25\Delta x,}{u_{max} + c_{max}}$$

where c_{max} is the maximum local wave speed, and the wave speed is defined as $c = (g'H)^{1/2}$. The algorithm (DENS20) maintained conversation of the original cloud mass. It lost less than 0.5% of the mass over the integration periods studied. Raithby (1976) suggests that upwind-difference schemes introduce damping due to transient behavior as well as spatial variations. Alternative schemes were examined, such as the flux-corrected-transport scheme of Book et. al. (1976) and the smoothing althorithm by P. E. Long; however the extra complication resulted in only small improvement in the results.

VALIDATION EXAMPLES:

The credibility of a numerical model depends upon its ability to reproduce accurately the values of plume size and concentration distribution found during field experiments. The field data selected for consideration include instantaneous releases of isothermal dense gases, LNG spills on water, and continuous releases of cold dense gases in the wind tunnel.

Slab Model Comparisons to Porton Downs Field Experiments:

The Porton Downs field trials used a gas source in the form of a cubical box of about 3.5 m side containing 40 m^3 of gas. The gas was released by allowing the sides of the box (made of thin pleated tarapulin material) to collapse to the ground under gravitational forces in about 0.8 seconds leaving a cube of the dense gas suddenly exposed to the prevailing wind conditions (Picknett, 1981). A total of 42 individual trials were run, covering a wide range of wind speeds, released gas density, surface roughness, atmospheric stability and ground slope. Measurements included visual records of plume outline as evidenced by tracer smoke and dosage and continuous concentration monitors. The gases released were mixtures of Freon (CCl_2Fl_2C) and air adjusted to specific gravities ranging from 1.2 to 4.2.

Hall, Hollis and Ishaq (1982) reproduced the behavior of Runs 3, 8, 21, 29, 33, and 37 from the Porton trials in a set of wind-tunnel experiments. In all cases they reproduced the time variation of plume width, plume shape, plume arrival and plume departure very well. There were very strong similarities between the field and model plumes. Comparisons were also made between field concentration measurements and the model measurements. Some of the comparisons showed very good agreement, but others were poor. Differences were attributed to the naturally occurring high levels of repeat variability and anomalies in the field measurements. (In some cases the data from integrated continuous monitors and dosage monitors varied by more than an order of magnitude.)

These same situations were calculated by the slab model. In each case the model replicated the Hallet al. behavior quite well and differed from the field data in the same manner that their tests did.

Porton trial 8 results are shown in Figures 1, 2, and 3. The field test was performed at wind speeds below the threshold values of the instruments available; hence the trial experiments was effectively in still air. Figure 1 displays peak concentrations measured at different downwind locations. Hall's model test, the slab model and a box model (Meroney and Lohmeyer, 1983) agree very well, but the field measurements do no seem to vary at all with distance. Figure 2 compares wind-tunnel, full scale, slab model, and box model cloud widths at various times from release. Agreement is excellent. Figure 3 displays concentration versus time traces at various radial locations. The slab model predicts Hall's wind-tunnel simulation of peak concentration, arrival time, and arrival of the maximum concentration very well. The larger concentrations and early arrival times found during the field test suggest that locally the wind was gusting and the average wind speed was not zero.

Slab Model Comparisons to China Lake Field Experiment:

During the Burro 8 Field Trial at China Lake Naval Weapons Center 28.4 m^3 of LNG was released at a rate of 16.0 m^3/min onto a small water pond. The wind speed was 1.8 $\pm$0.3 m/sec and decreasing at a 1 m height, while the atmospheric stability was slightly stable. Humidity was measured to be 5% upwind of the spill and air temperature was 33^{o}C. Since the plume mixed violently over the pond it is likely that humidity downwind of the pond is higher (say 20%). This spill displayed the most gravity dominated behavior of those performed. (See Koopman, et al. (1982) and Meroney and Neff (1981) for a discussion of field data.)

The slab model described earlier was run for Burro 8 initial conditions for a) adiabatic entrainment of dry air and b) mixed convection heat transfer and entrainment of air at 20% humidity. The maximum concentrations of methane, C_m, versus downwind distance, x, is plotted in Figure 4. Both predictions are well within the scatter of the field data. Water vapor condensation and heat transfer initially result in somewhat accelerated dilution out to 150 m; however subsequent re-evaporation of condensed water vapor re-cools the plume and the two curves rejoin one-another. Although the effect of heat transfer and humidity are to accelerate entrainment, they also reduce the plume lateral spread significantly as shown in Figure 5. This reduction of plume surface area seems to compensate for any increased entrainment rate; hence plume concentrations are only slightly modified by heat transport. Since the wind speeds involved in Burro 8 are quite small and the boil off times short calculations were performed assuming that the entire volume was released instantaneously and then repeated with the boiloff spread over the observed release time. Plots of the transient behavior of the LFL mean concentration of 5% are displayed in Figure 6 and 7.

A cross-section of plume concentrations at x = 140 m at a time after release of 200 sec is show in Figure 8. These isopleths were created from the predicted slab data for plume height, width, and centerline concentrations by distributing the plume in the manner suggested by Ermak et al. (1982) where, $\bar{C}_m(x,y,z)=\bar{C}_m(x,o,o)\{1-(2y/3B)^2\}\cdot\{1-(2z/3H)^2\}$. Measured isopleths are plotted in the same figure for comparison. The slab model can not reproduce the lateral varia-

tions in plume height and circulation associated with gravity heads and horseshoe vortices.

Slab Model Comparison to CSU Cold Gas Wind-Tunnel Experiments:

A cold dense plume measurement program was performed to provide a basis for the analysis of heat transfer effects of plume dispersion by Andreiev, Neff, and Meroney (1983). Plumes were released continuously from a constant-area ground-level source in a simulated atmospheric boundary layer. Source gas mixtures were prepared to proved gases which were all initially heavy, but they were either isothermal, cold with source specific heat capacity equal to that of air, or cold with source specific heat capacity greater than that of air. Thus one could evaluate whether dilution resulted from adiabatic entrainment mechanisms, heat transfer effects, or unbalanced thermal expansion. Two buoyancy conditions were examined such that bouyancy length scales equalled ℓ_b = 1.0 to 8.0 cm, but source conditions were selected to maintain Flux Froude number equality among cases. Gases released included CCl_2Fl_2-air mixtures, cold nitrogen, cold carbon dioxide, and cold methane. Tests at laboratory scales exaggerate heat transfer effects; therefore duplication of the plume behavior by a numerical model is an extreme test for any model. Figure 9 shows a selection of cold plume data in terms of the along-wind decay in dimensionless concentration coefficient, $K = \bar{C}_m U_R H_o^2 T_a / (T_o Q(1-C))$. Heat transfer effects result in increased decay rate as ℓ_b increases (i.e. smaller source flow rate or decreased wind speed).

The slab model was used to predict K behavior over equivalent source and flow conditions. Comparison of Figures 9 and 10 reveal very

Figure 14 displays similar plots for the less dense cloud. In this case very little upwind movement occurs. The cloud moves only one cloud height upwind and then retreats downwind. The cloud attempts to send another gravity head upwind, but this again fails, and finally the cloud moves downwind as a semicircular cloud. The concentration curves suggest that, although larger relative velocities exist on the upwind side, there is relatively less surface over which to entrain. The greater cloud surface downwind presents an opportunity for more dilution even though it occurs at a smaller rate per unit area. Thus the concentration curves in Figures 13 and 14 slump in opposite directions.

Gravity Waves on the Upper Cloud Surface:

Plots of plume height, H/HI, versus radial location, R/RI, from a radially symmetric slab model calculation reveal an interesting cloud surface phenomenon. Figures 15 and 16 display progressive cloud profiles for calm and 0.2 m/sec wind speed conditions. The depth-averaged equations produce the appearance of a gravity head at early times; however, an elevated cloud nose cannot be produced by a depth-averaged approach. Notice that the long time cloud height is nearly constant with radius and time for low wind speeds. The cloud grows more rapidly for finite wind speed conditions, because shear layer turbulence permits growth at a rate $v_g \sim u_*$, rather than $v_g \sim 1/R$.

Surface waves develop on the cloud top after about $t^* = 30$. One's first reaction might be that these waves are evidence of numerical instability; however they are actually a real phenomenon. Sketched on Figure 7 are typical plots of local radial density, ρ, and the cloud height, H at some time greater than $t^* = 30$. Also displayed is the

similar behavior. Figures 11 and 12 compare equivalent methane molar concentration decay with downwind distance to slab model predictions. Agreement is excellent.

The slab model is seen to reproduce the essence of dense cloud behavior for isothermal or cold dense clouds released suddenly, over a finite time, or continuously. Now that model credibility is established it is appropriate to examine various aspects of the plume physics questions posed in the introduction.

NUMERICAL PREDICTION OF DENSE CLOUD PHYSICS:

Versions of the slab problem designed to run in two-dimensional, radial, or laterally symmetric were used as appropriate to illuminate the dense cloud physics. The following sections examine each point in order.

Upwind Motion and Breaking of the Head Wave:

A two-dimensional version of the slab model was used to examine the effects of an opposing wind on the upwind cloud front. A two-dimensional square container of isothermal dense gas was released suddenly. Two cases are examined one for SG = 4.17 and one for SG = 1.2 while maintaining the same approach flow.

Figure 13 displays the variation of the dense gas cloud height ratio, H/HI, and concentration versus longitudinal location, X/HI, with time, t^*. The cloud initially surges upwind, deepens at the upwind front as a result of the opposing fluid field and then shifts downwind. At long times the height distribution becomes symmetric about the cloud center. More dilution takes place at the upwind edge of the cloud where the relative velocity of the wind about the cloud is greater.

product ρH^2 which is the hydrostatic pressure. The product term has a maximum, which means fluid to the left of the maximum will be accelerated toward cloud center, while fluid to the right of the center will be accelerated outward. The result is fluid moving toward cloud center as shown in the second sketch. As fluid piles up at the cloud center it produces local wavespeed conditions which exceed the average fluid velocities and a series of waves move outward. These waves grow in time as they induce additional pressure perturbations, high local velocities, and greater entrainment rates. The typical progression of cloud shapes calculated are shown at the bottom of Figure 17.

Picknett (1981) reported the presence of gravity waves during the Porton experiments. He notes:

> "Of special interest is the consistency in cloud height after the initial violent motion has subsided. ...In this slow expansion phase the surface of the disc of cloud is sometimes disturbed by regular undulations, 100-200 mm in amplitude, several meters in wavelength and traveling at perhaps 200 mms^{-1}, which may, perhaps, be gravity waves."

Picknett also commented on the "surprising" rate of cloud dilution after initial cloud collapse for such a low wind speed. He attributed this mixing to persistent cloud turbulence possibly aided by the gravity waves.

Source Behavior During Instantaneous, Finite Time, and Continuous Gas Release:

During the comparison of the slab model with the Burro 8 field test Figures 5 and 6 compared the lateral cloud growth effect of releasing the cloud suddenly and over the observed finite time period. The cloud might also be considered to boiloff continuously from an extended spill of LNG onto water. Figure 18 indicates the spread associated with such

a supposition. During the sudden release scenario the cloud almost immediately convects downwind, but during the finite time release the 5% isopleth is bound to the source until the end of the release time, whereas the 5% isopleth becomes parabolic with an open end downwind during a continuous situation. The continuous release appears most hazardous in terms of downwind advection of flammable gas; however the instantaneous release results in the widest plume isopleth.

Shape of Transient Ignition Zones:

Meroney and Lohmeyer (1983b) studied the statistical characteristics of dense gas clouds released in an atmospheric-boundary-layer wind tunnel. They found that the maximum root-mean-square of the concentration fluctuations (standard deviation) could be related to the local mean concentration by $\overline{c'^2}/\overline{C}_m^2 = 0.02/\overline{C}_m$. In addition the concentration, C_m, may be considered distributed in a log-normal manner at low concentrations. Thus knowledge of the mean concentration, standard deviation, and probability distribution permits calculation of the ignition probability of gas, P. (P is the likelihood that a flammable gas mixture will exist at a given location during any instant of a dense gas spill.)

Table 1 proposes hazardous zones for the three release cases discussed in the section above. Naturally the hazard zones are most extensive for situations where the mean concentration is advected the greater distances. These predictions of hazard zones are still conservative because of the conservative nature of the standard deviation algorithm used.

Table 1. Distances to Lower Flammability Limit Based on Mean Concentration or P ignition = 0.05, for Burro Run No. 8

Source Condition	$\bar{C}_m$ = 0.05		P ignition = 0.05	
	x_{LFL} (m)	t_a (sec)	x_{LFL} (m)	t_a (sec)
Field Data	340	200	---	---
Sudden Release (DENS 20)	330	130	657	280
Finite Time Release w_o = 0.098 m/s t_R = 107 sec (DENS 20)	280	180	650	330
Continuous Release w_o = 0.098 m/s (DENS 20)	280	180	653	355

All numerical calculations with surface heat transfer by mixed convection and 7% relative humidity.

Acknowledgements:

The author wishes to acknowledge support from the Institute Wasserbau III, University of Karslruhe, F. R. G.; the von Humboldt Foundation, F. R. G.; and the Gas Research Institute, U. S. A.

REFERENCES:

Andreiev, G., Neff, D. E.,and Meroney, R. N. (1983), Heat Transfer Effects During Cold Dense Gas Dispersion, Gas Research Institute Report No. GRI83/_____, _____pp.

Book, D. L., Borris, J. P. and Hain, K. (1976), Flux Corrected Transport III: Minimal-error FCT Algorithms, J. Comp. Phys., Vol. 20, pp. 397-431.

Britter, R. E. and Griffiths, R. F. (editors), (1982), Dense Gas Dispersion, Elsevier Scientific Publishing Company.

Ermak, D. L., Chan, S. T., Morgan, D. L., and Morris, L. K. (1982), A Comparison of Dense Gas Dispersion Model Simulations with Burro Series LNG Spill Test Results, J. Hazardous Materials, Vol. 6, Nos. 1 and 2, pp. 129-160.

Hall, D. J., Hollis, E. J., and Ishaq, H. (1982), A Wind Tunnel Model of the Porton Dense Gas Field Trials, Warren Springs Laboratory Report L394(AP), Dept. of Industry, Stevenage, Hertfordshire, U. K., 106 pp.

Koopman, R. P., Cederwall, R. T., Ermak, D. L., Goldwire, H. C. Jr., Hogan W. J., McClure, J. W., McRae, T. G., Morgan, D. L., Rodean, H. C., and Shinn, J. H. (1982), Analysis of Burro Series 40 m^3 LNG Spill Experiments, J. of Hazardous Materials, Vol. 6, Nos. 1 and 2, pp. 43-84.

Meroney, R. N. (1983), Unsteady Behavior of a Simulated LNG Vapor Cloud Suddenly Released into a Wind-tunnel Boundary Layer, Proceedings of American Gas Association Transmission Conference, May 2-4, 1983, Seattle, Washington, 21 pp.

Meroney, R. N. and Lohmeyer, A. (1982), Gravity Spreading and Dispersion of Dense Gas Clouds Released Suddenly into a Turbulent Boundary Layer, Gas Research Institute Research Report GRI-81/0025, Chicago, Illinois, U. S. A., 220 pp.

Meroney, R. N. and Lohmeyer, A. (1983a), Prediction of Propane Cloud Dispersion by a Wind-tunnel-data Calibrated Box Model, accepted by J. Hazardous Materials, 33 pp.

Meroney, R. N. and Lohmeyer, A. (1983b), Statistical Characteristics of Instantaneous Dense Gas Clouds Released in an Atmospheric Boundary Layer Wind Tunnel, Submitted to J. Boundary-Layer Meteorology, 38 pp.

Meroney, R. N. (1983), Prediction of Propane Cloud Dispersion by a Wind-tunnel-data Calibrated Box Model, J. of Hazardous Materials, accepted for publication, 33 pp.

Meroney, R. N. and Neff, D. E. (181), Physical Modeling of Forty Cubic Meter LNG Spills at China Lake, Caliornia, Air Pollution Modeling and Its Applications, Vol. 1, edited by C. de Wispelaere, Plenum Publishing Corp., pp. 24-27.

Picknett, R. G. (1981), Dispersion of Dense Gas Puffs Released in the Atmosphere at Ground Level, Atmospheric Environment, Vol. 15, pp. 509-525.

Raithby, G. D. (1976), A Critical Evaluation of Upstream Differencing Applied to Problems Involving Fluid Flow, Computer Methods in Applied Mechanics and Engineering, Vol. 9, pp. 75-103.

LIST OF SYMBOLS:

Symbols	Definitions
C	Concentration
C_m	Maximum transient concentration
C_{med}	Median concentration
C_1, C_2	Lower and upper flammability limits
c	Concentration fluctuation
g'	Modified gravitational constant
Ri_*	Richardson number
T	Time scale
t	Time
U	Velocity scale
u	Velocity
u_*	Friction velocity
x	Downwind distance
X	Concentration
σ_1	Log-normal standard deviation
ϕ	Humidity
Subscripts	
a	Arrival time
i	Initial
d	Departure time
m	Maximum
o	Ground level
R	Reference
Superscripts	
$\overline{\quad}$	Ensemble average
*	Dimensionless

LIST OF FIGURES

Tables

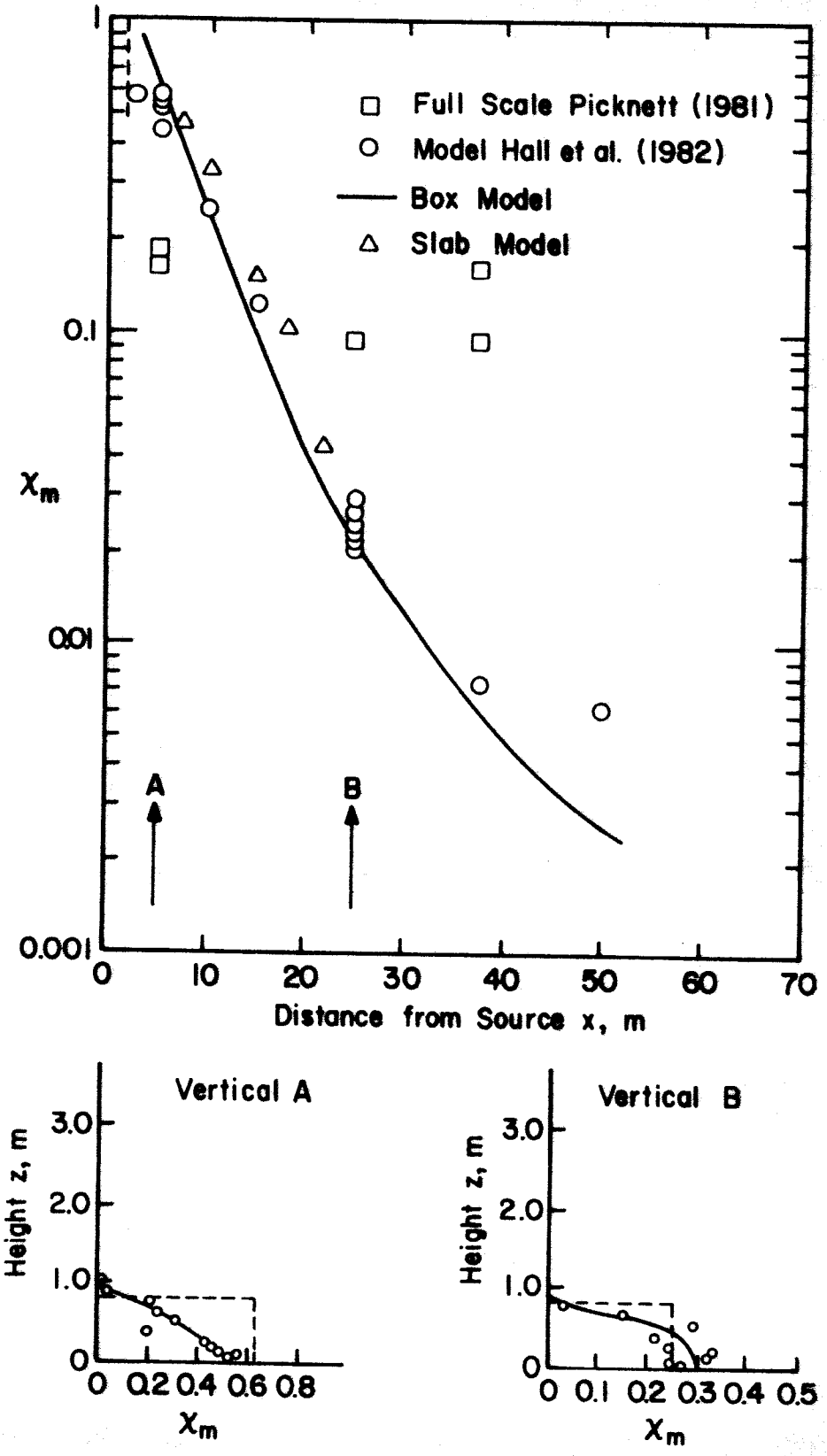

Figure 1. Porton Trial No. 8 - Peak Concentrations in Cloud

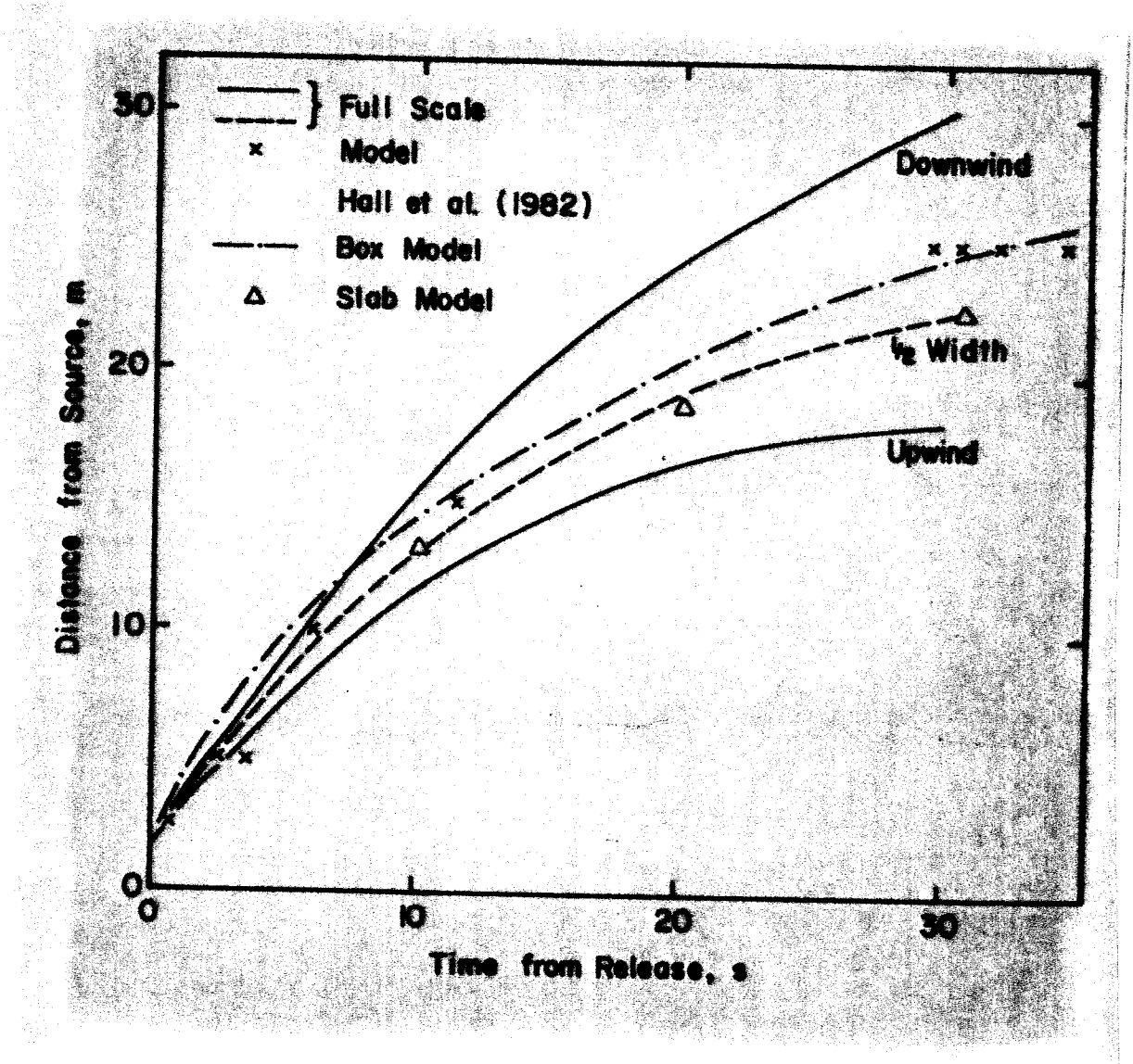

Figure 2. Porton Trial No. 8 - Cloud Size Variation

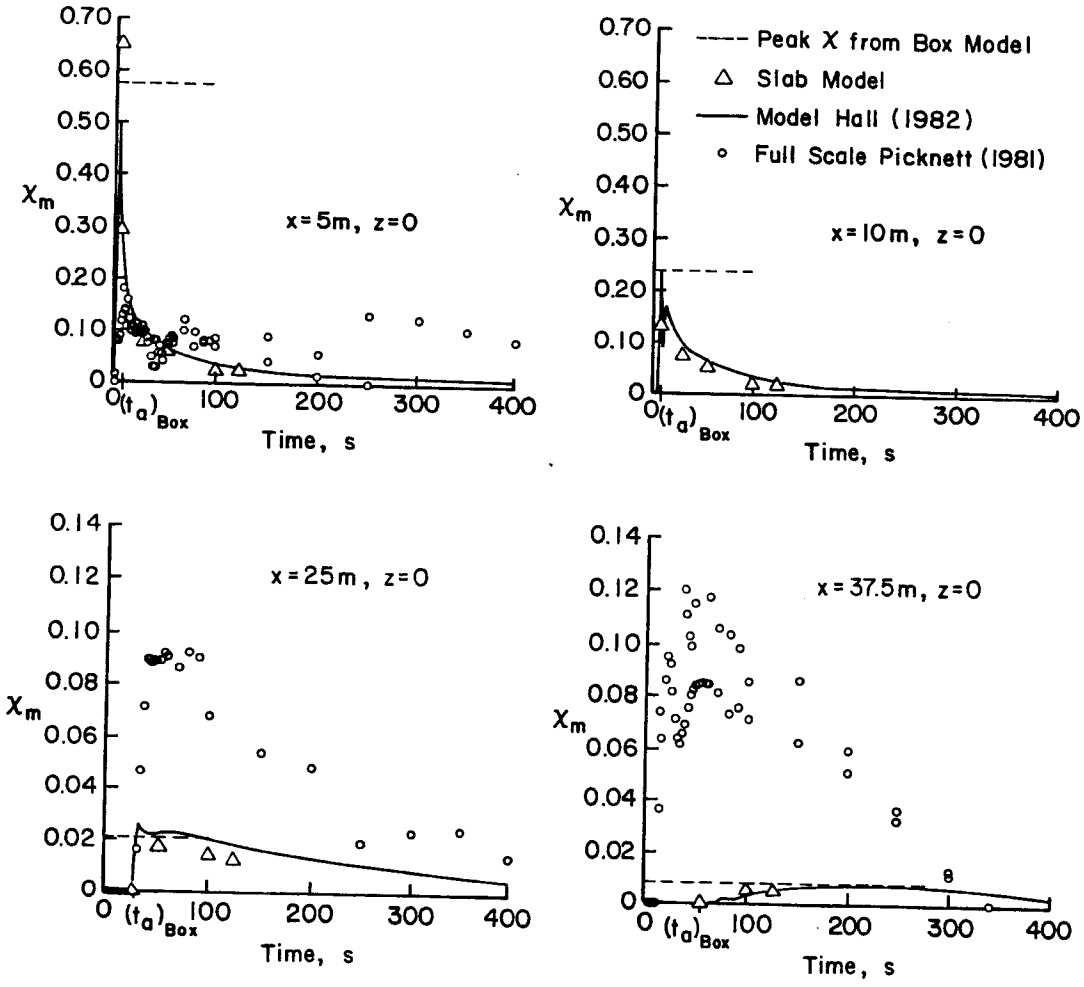

Figure 3. Porton Trial No. 8 - Continuous Monitor Measurements

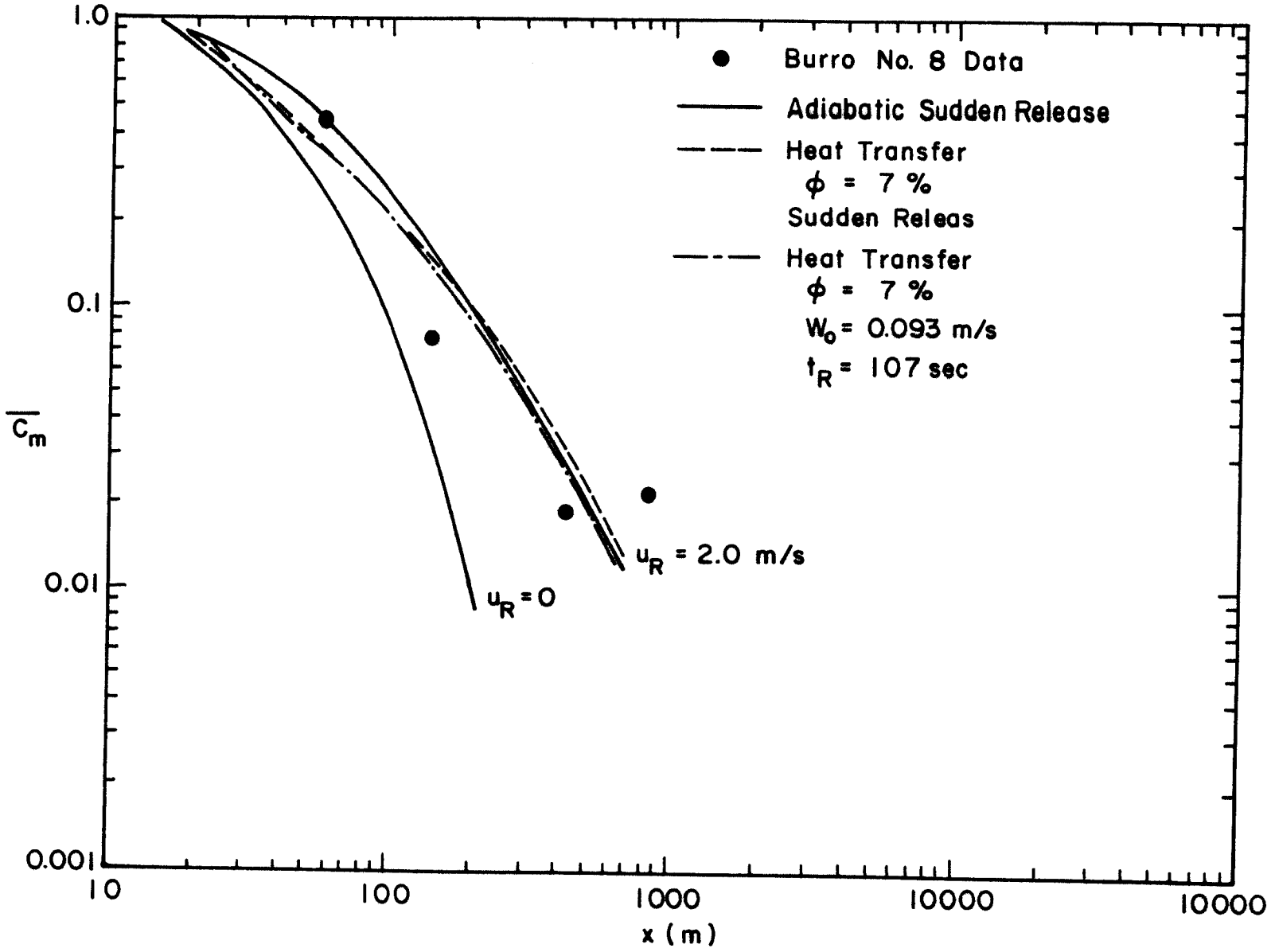

Figure 4. Burro Trial No. 8 - Peak Concentrations at Ground Level

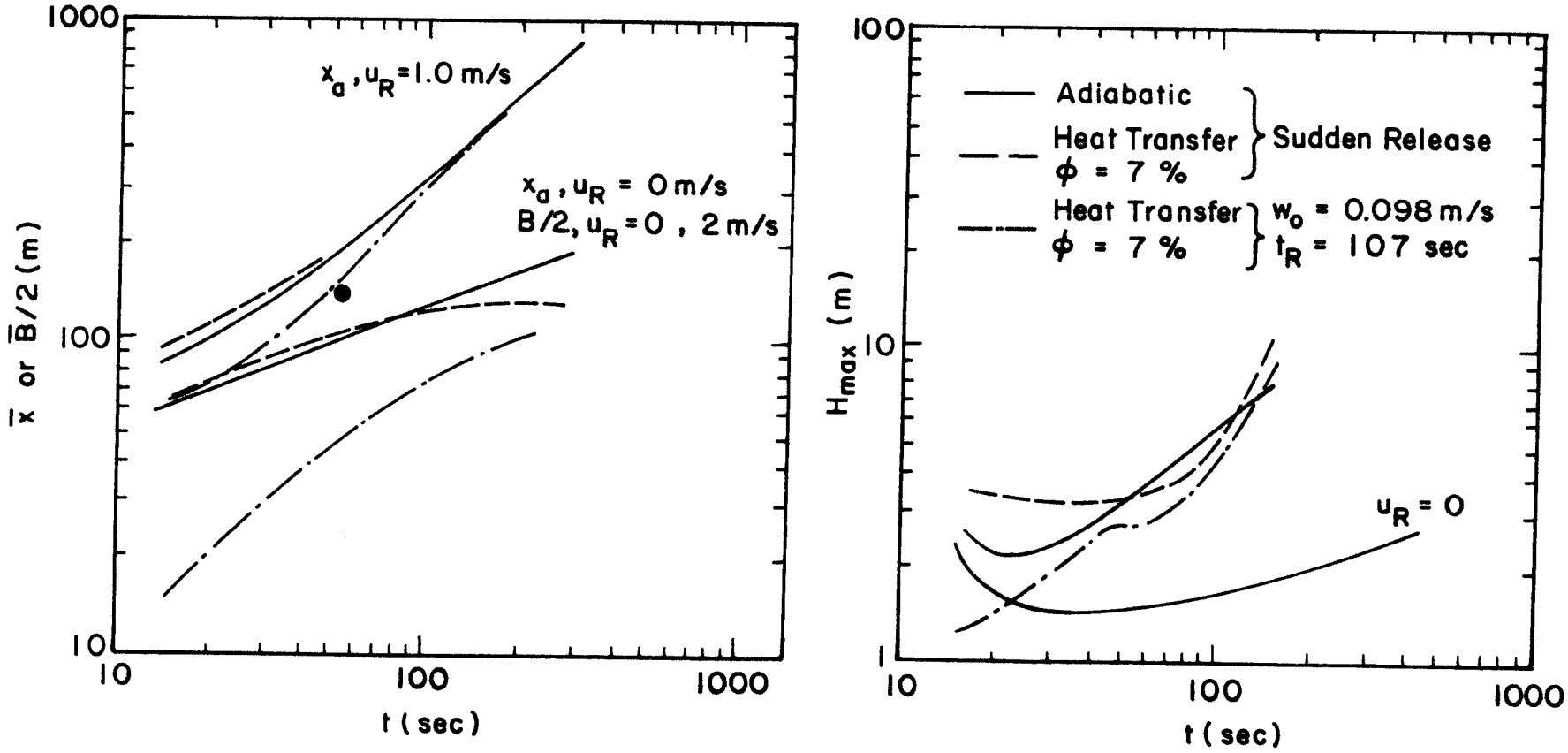

Figure 5. Burro Trial No. 8 - Cloud Size Variation

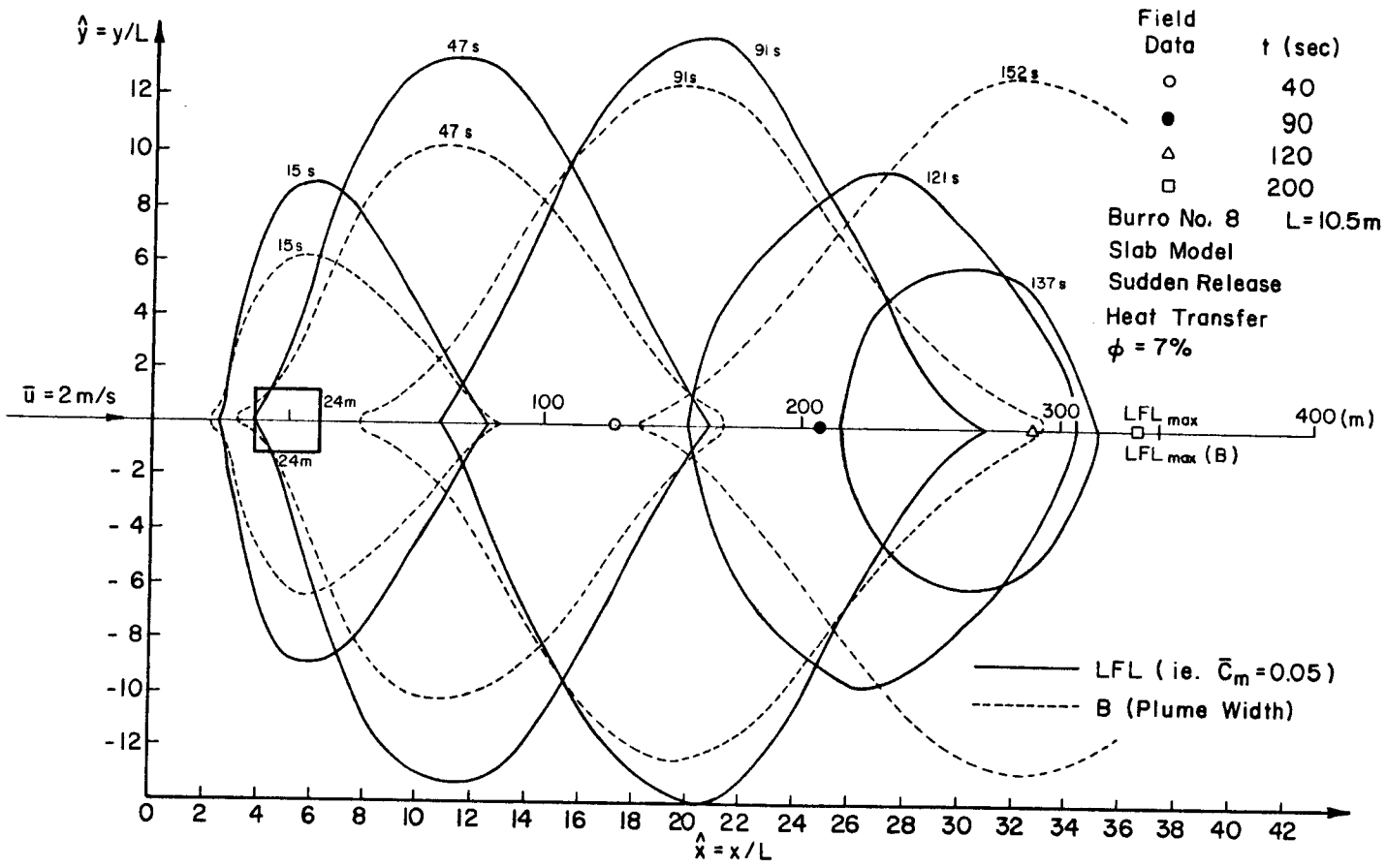

Figure 6. Burro Trial No. 8 - Transient Behavior of the LFL Mean Concentration of 5% Sudden Cloud Release

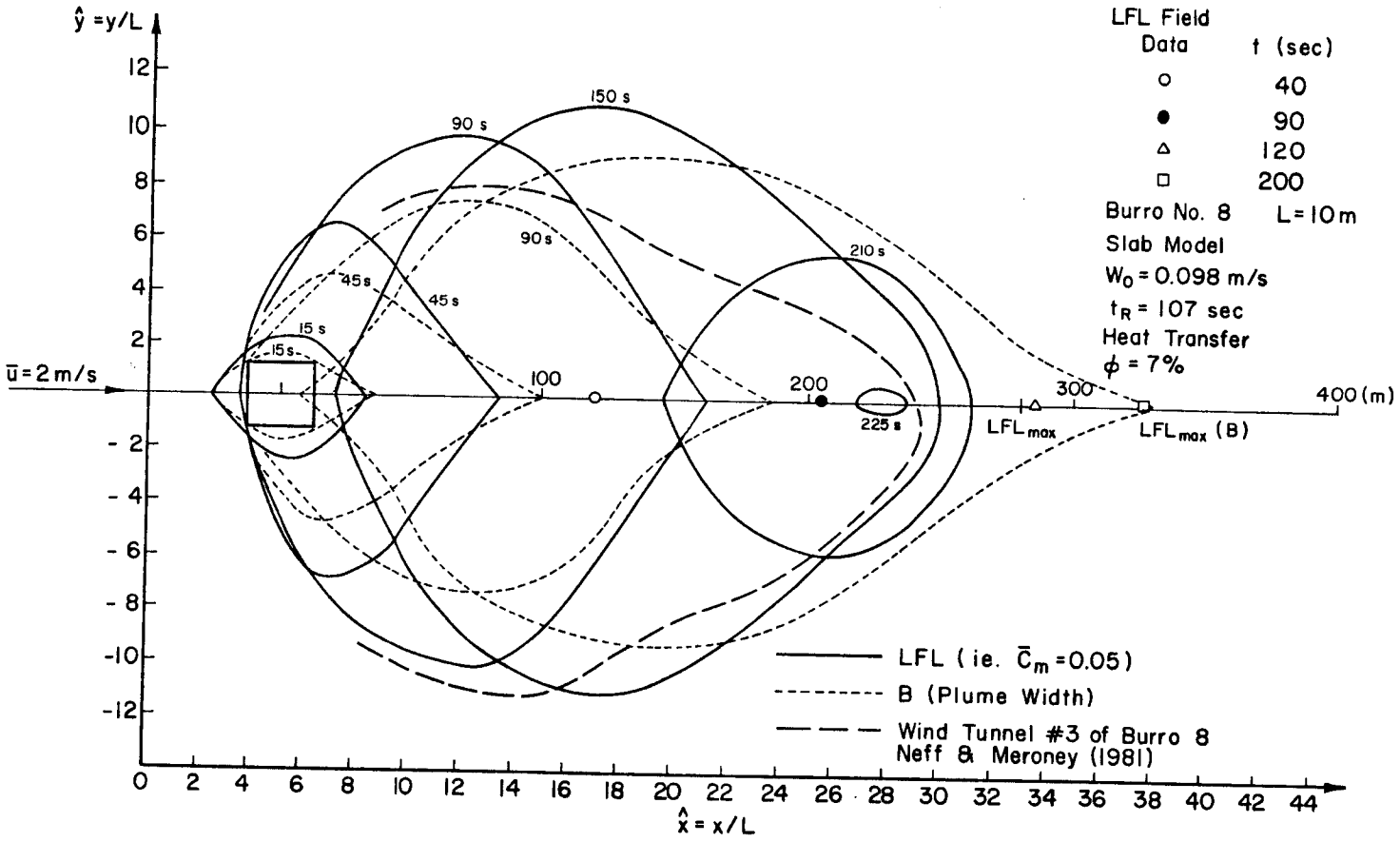

Figure 7. Burro Trial No. 8 - Transient Behavior of the LFL Mean Concentration of 5% Finite Boiloff Time

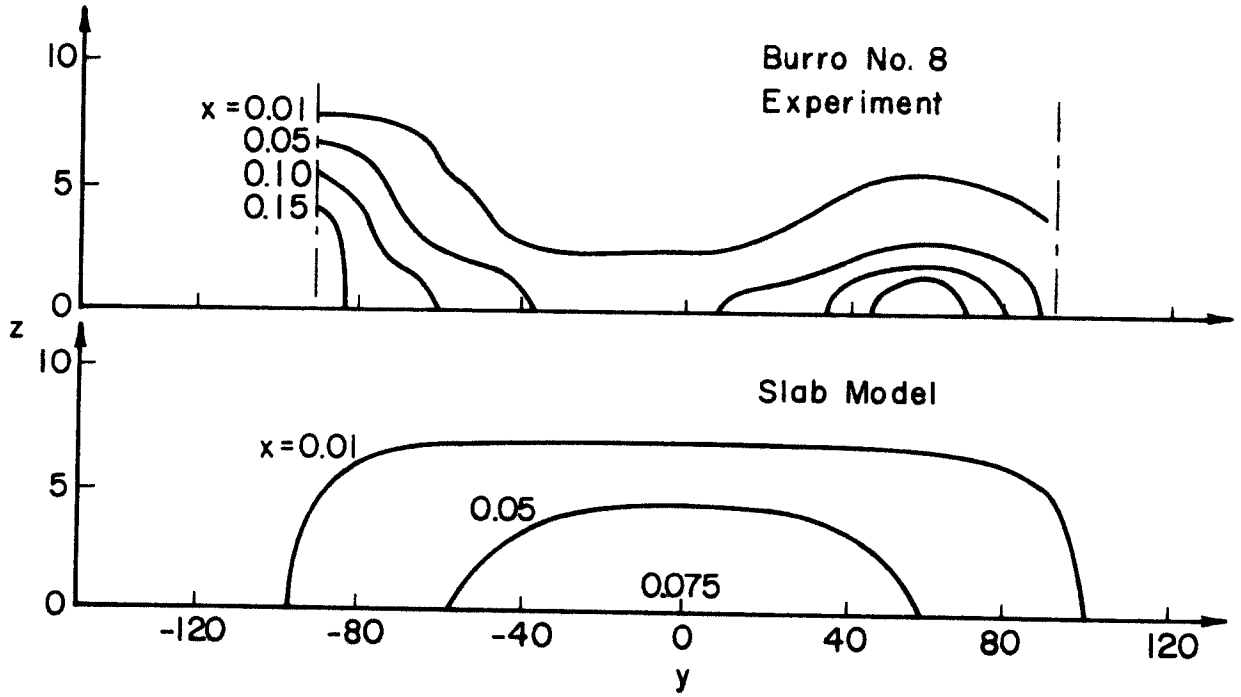

Figure 8. Burro Trial No. 8 - Concentration Cross-section at 140 m at 200 sec

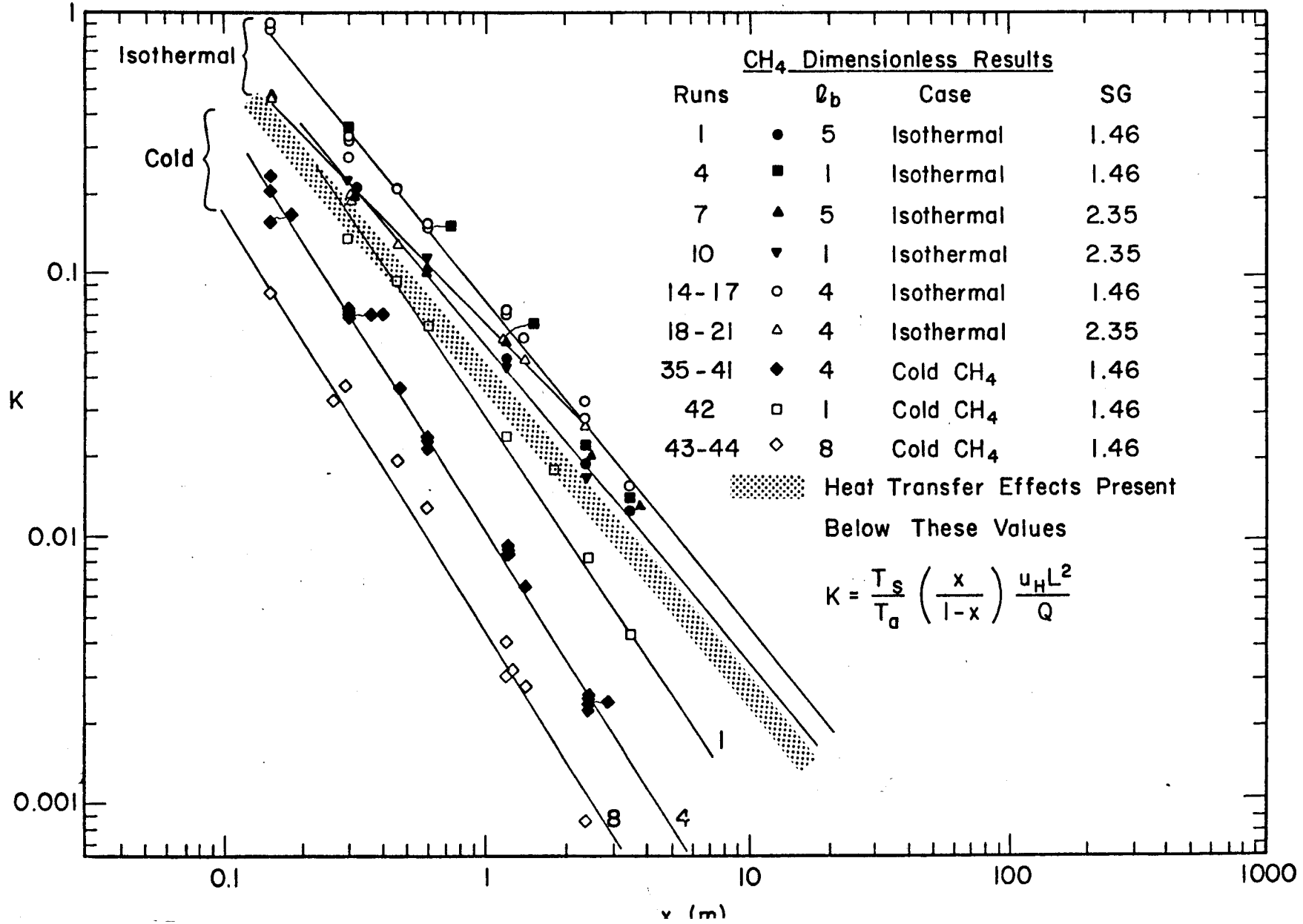
Isothermal
Cold
CH4 Dimensionless Results
Runs
ℓb
Case
SG
1 ● 5 Isothermal 1.46
4 ■ 1 Isothermal 1.46
7 ▲ 5 Isothermal 2.35
10 ▼ 1 Isothermal 2.35
14-17 ○ 4 Isothermal 1.46
18-21 △ 4 Isothermal 2.35
35-41 ◆ 4 Cold CH4 1.46
42 □ 1 Cold CH4 1.46
43-44 ◇ 8 Cold CH4 1.46
Heat Transfer Effects Present Below These Values
K = (Ts/Ta)(x/(1-x))(uHL²/Q)
K
x (m)
1
0.1
0.01
0.001
0.1
1
10
100
1000
8
4
1

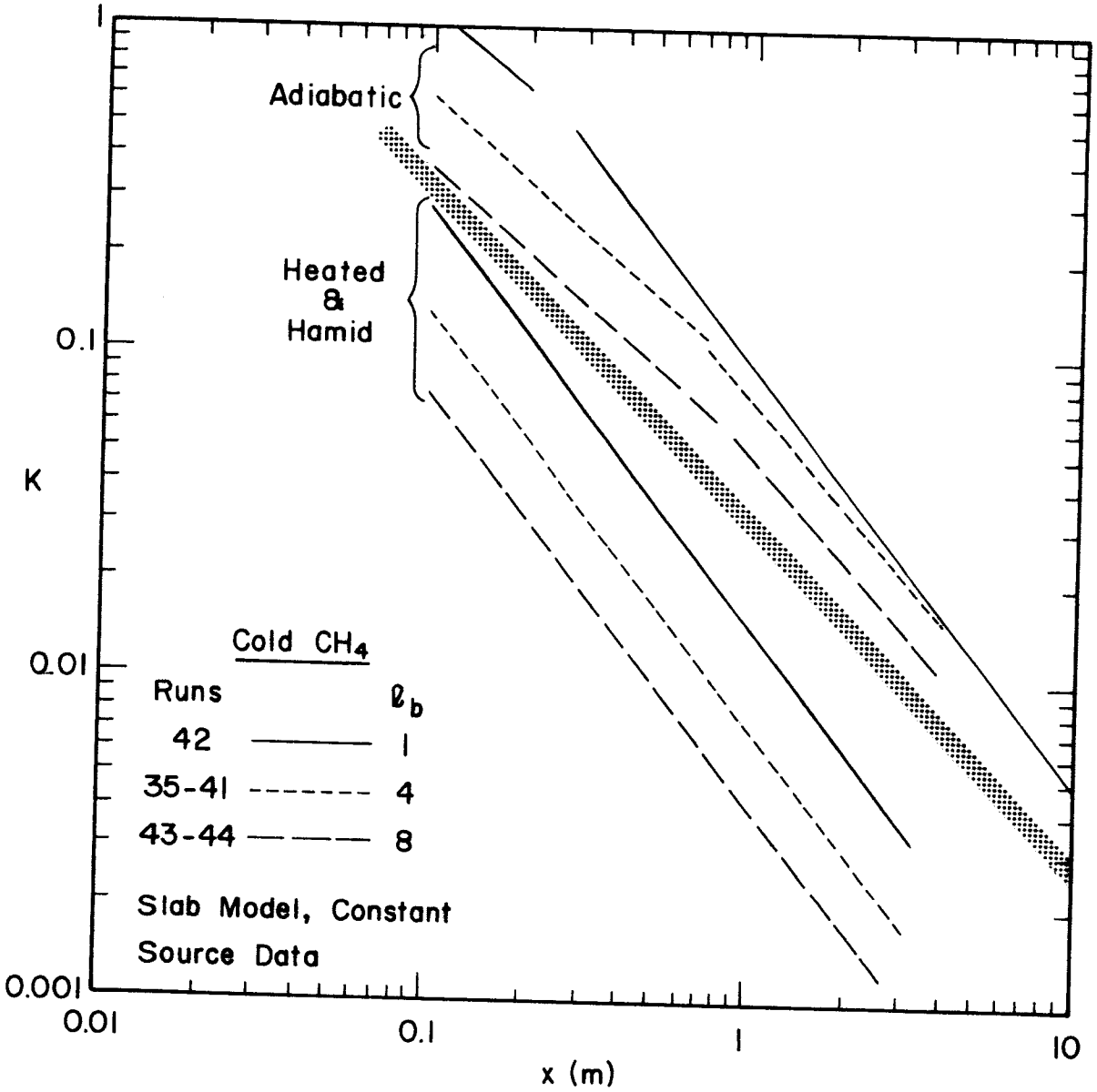

Figure 10. Cold Dense Gas Concentration Coefficient, K versus Down-wind Distance - Numerical Prediction

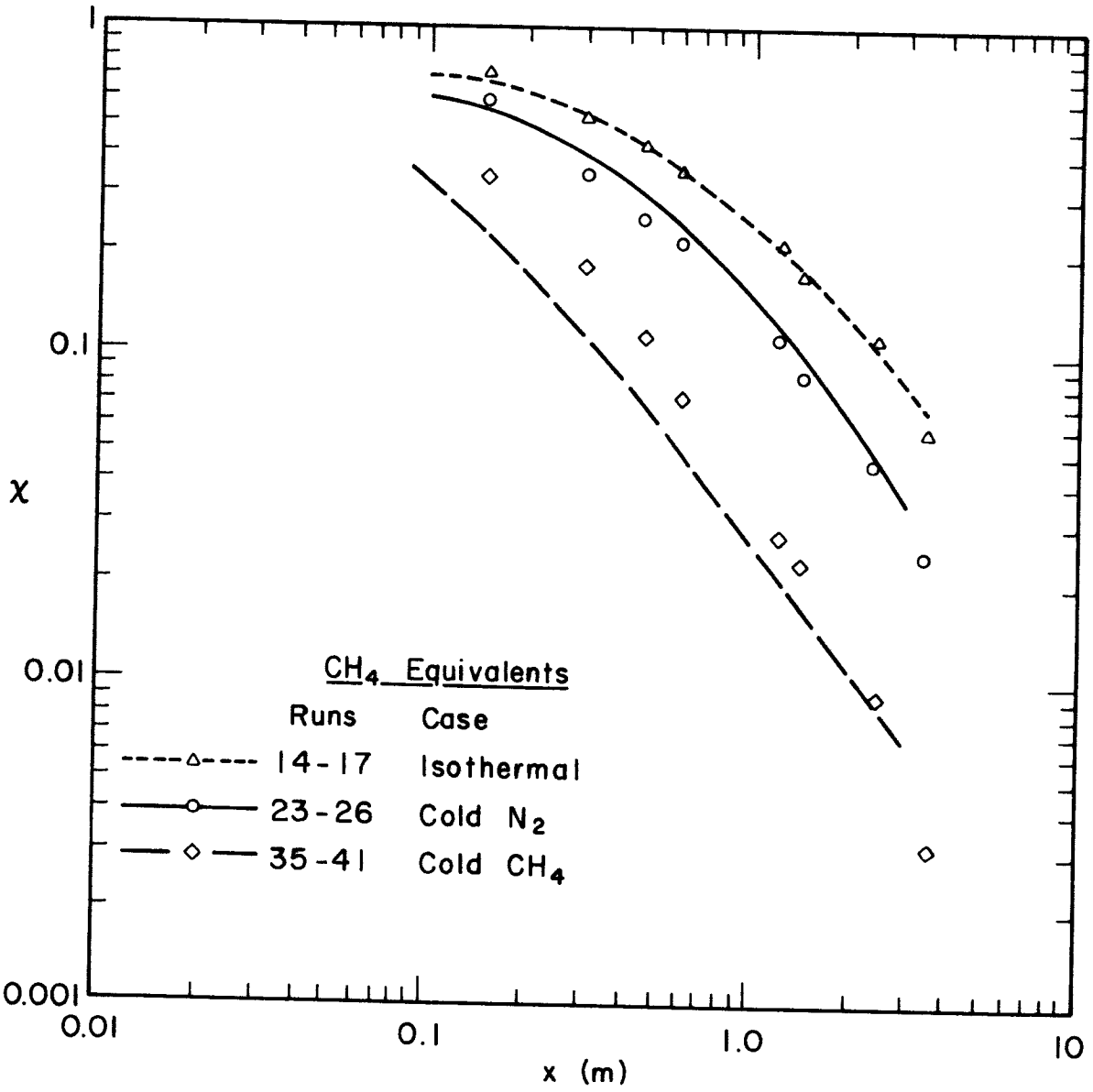

Figure 11. Concentration Decay with Down-wind Distance - Data and Numerical Predictions, Runs 14-17, 23-26, and 35-41, ℓ_b = 4 cm

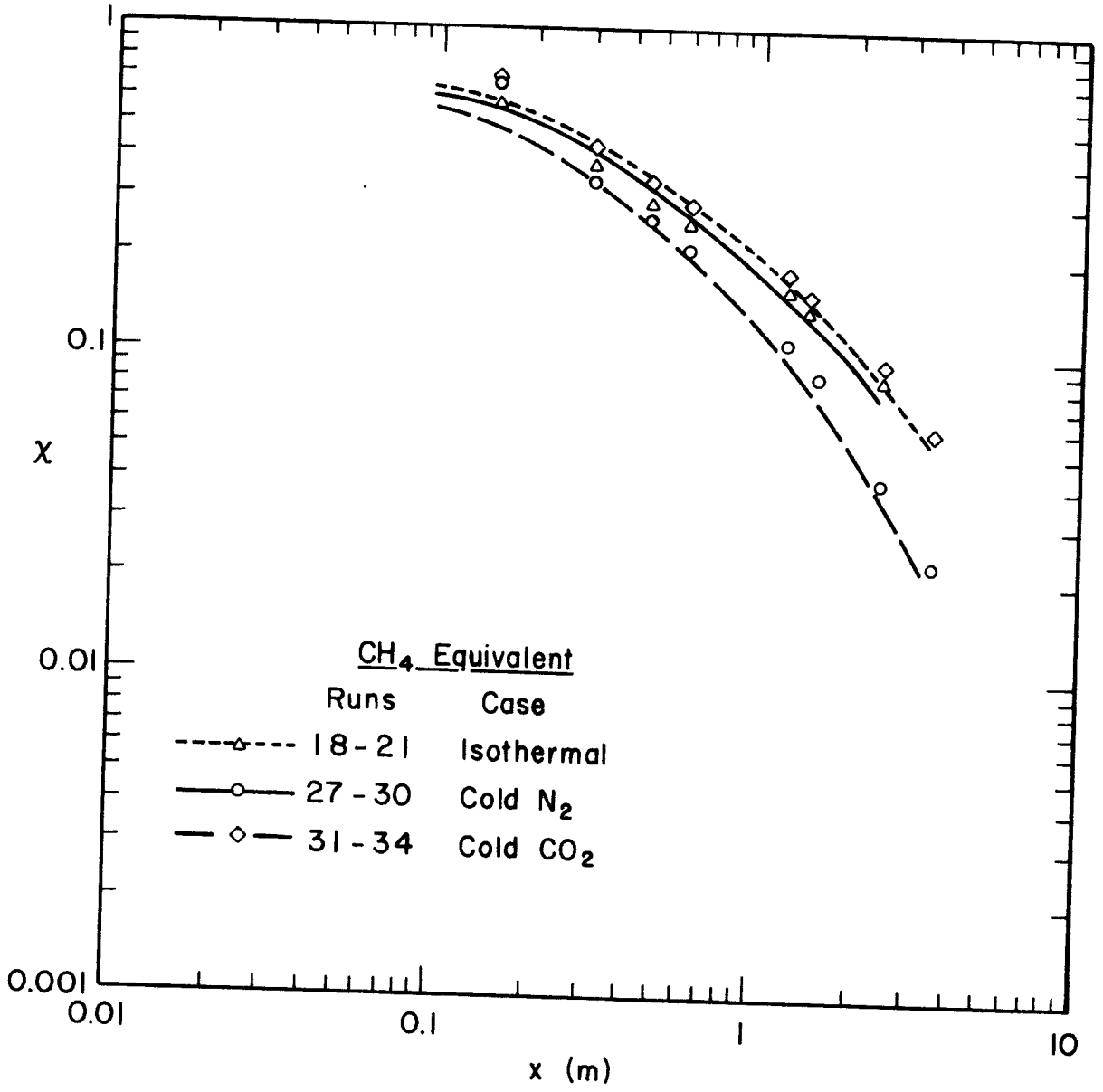

Figure 12. Concentration Decay with Down-wind Distance - Data and Numerical Predictions, Runs 18-21, 27-30, and 31-34, ℓ_b = 1 cm

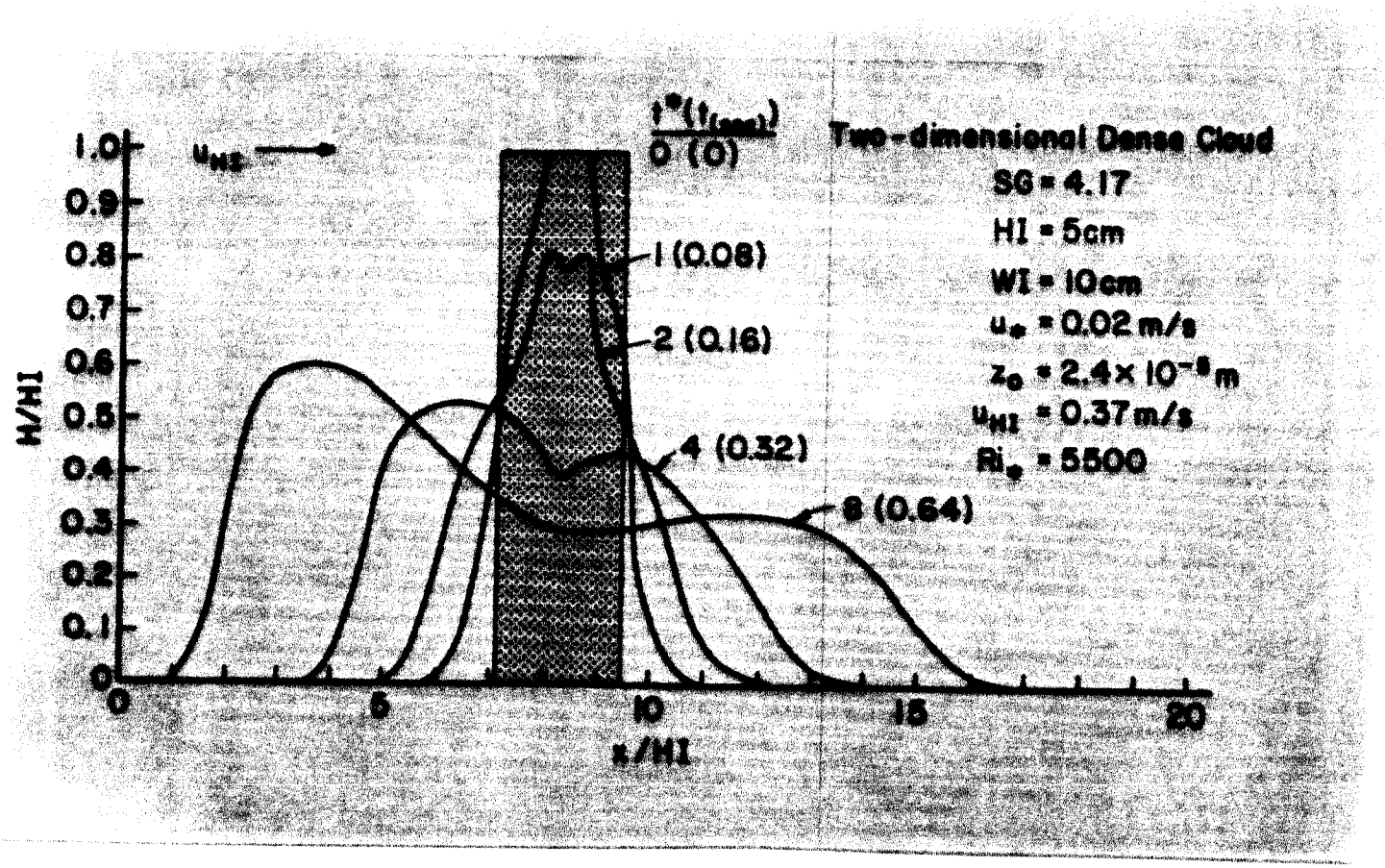

Figure 13a. Transient 2-D Cloud Growth, SG = 4.17, u_R = 2 cm/sec, Ri_* = 5500

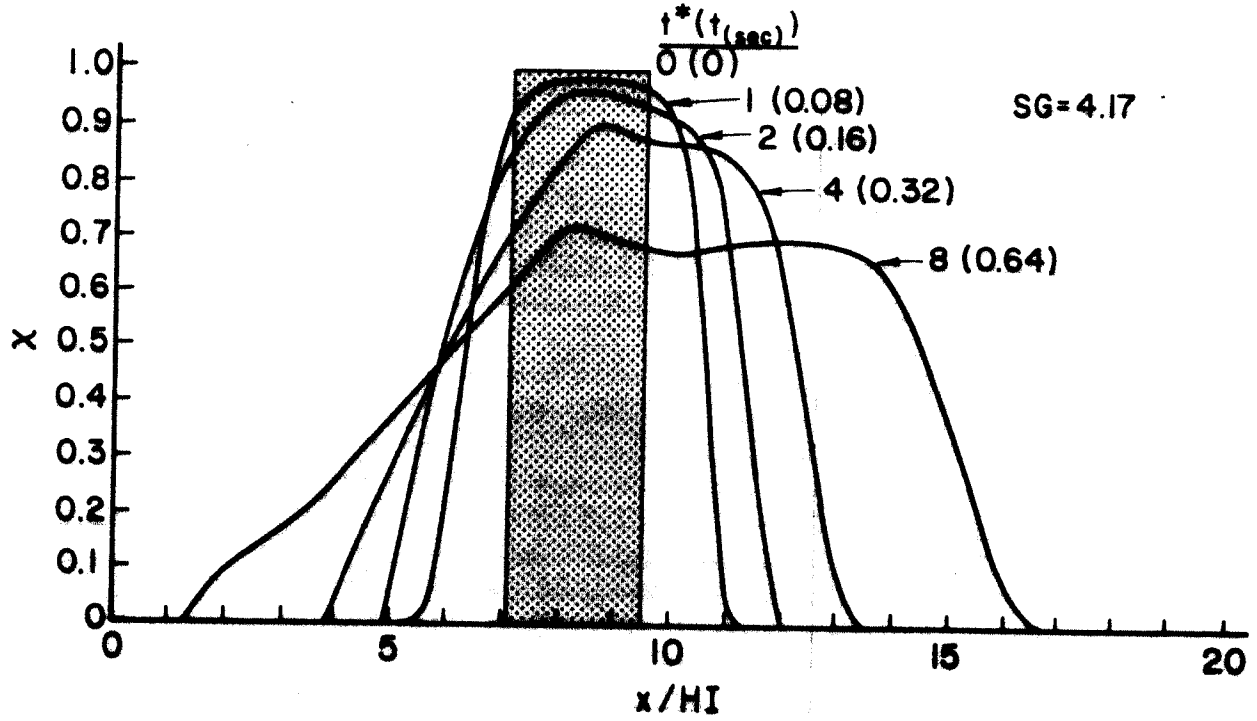

Figure 13b. Transient 2-D Cloud Growth, SG = 4.17, u_R = 2 cm/sec, Ri_* = 5500

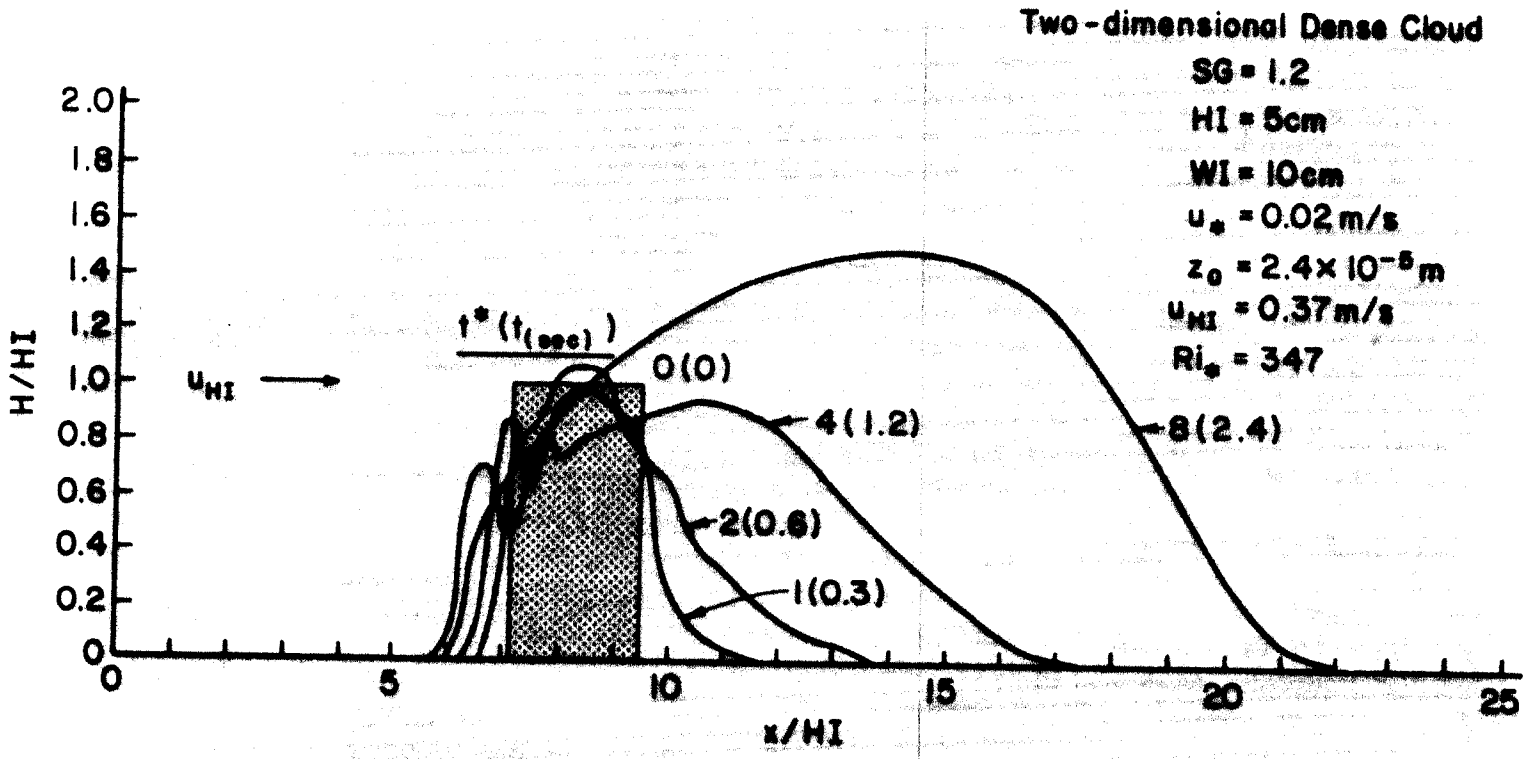

Figure 14a. Transient 2-D Cloud Growth, SG = 1.2, u_R = 2 cm/sec, Ri_* = 347

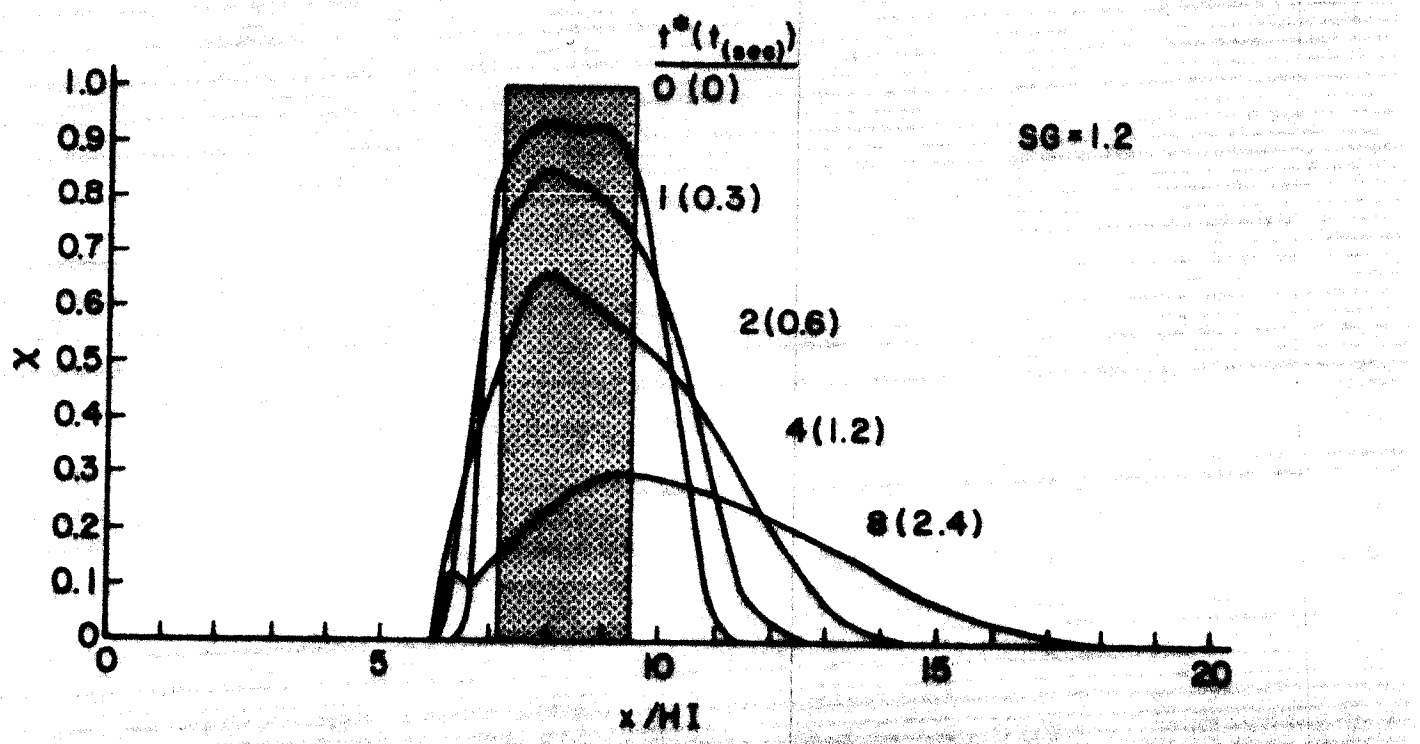

Figure 14b. Transient 2-D Cloud Growth, SG = 1.2, u_R = 2 cm/sec, Ri_* = 347

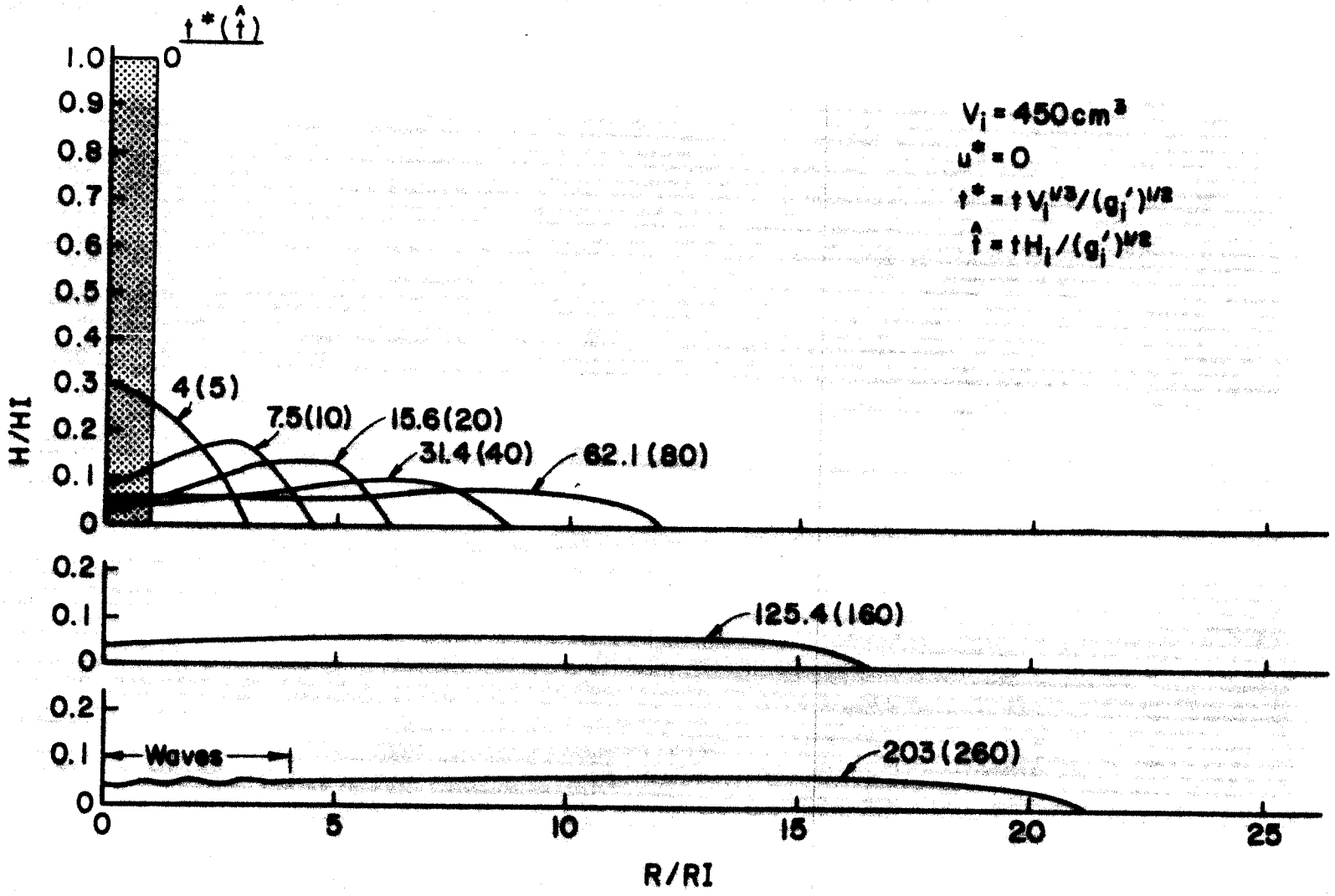

Figure 15. Cloud Height, H/HI, versus Radius, R/RI, $Ri_* = \infty$

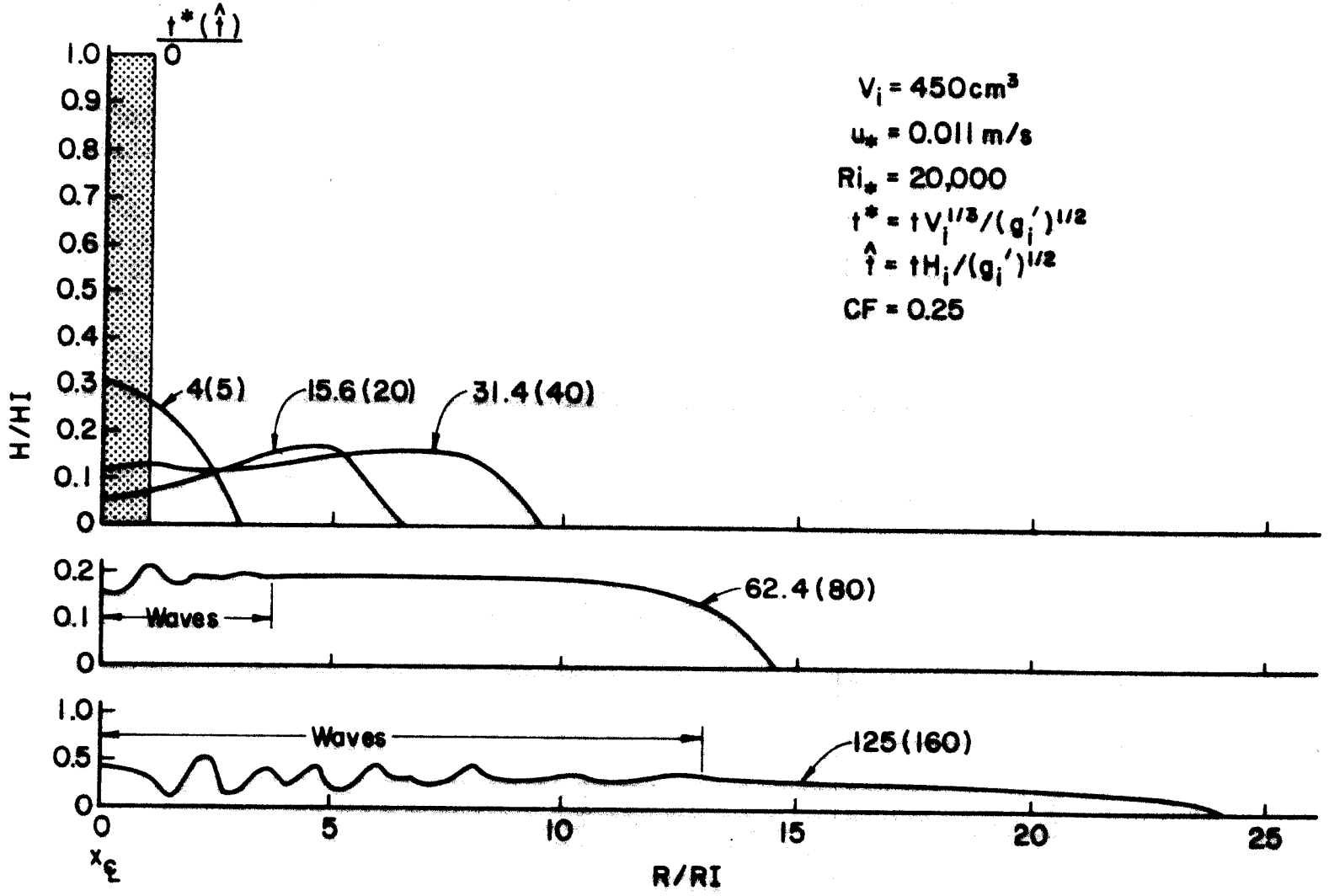

Figure 16. Cloud Height, H/HI, versus Radius, R/RI, $Ri_* = 20,000$

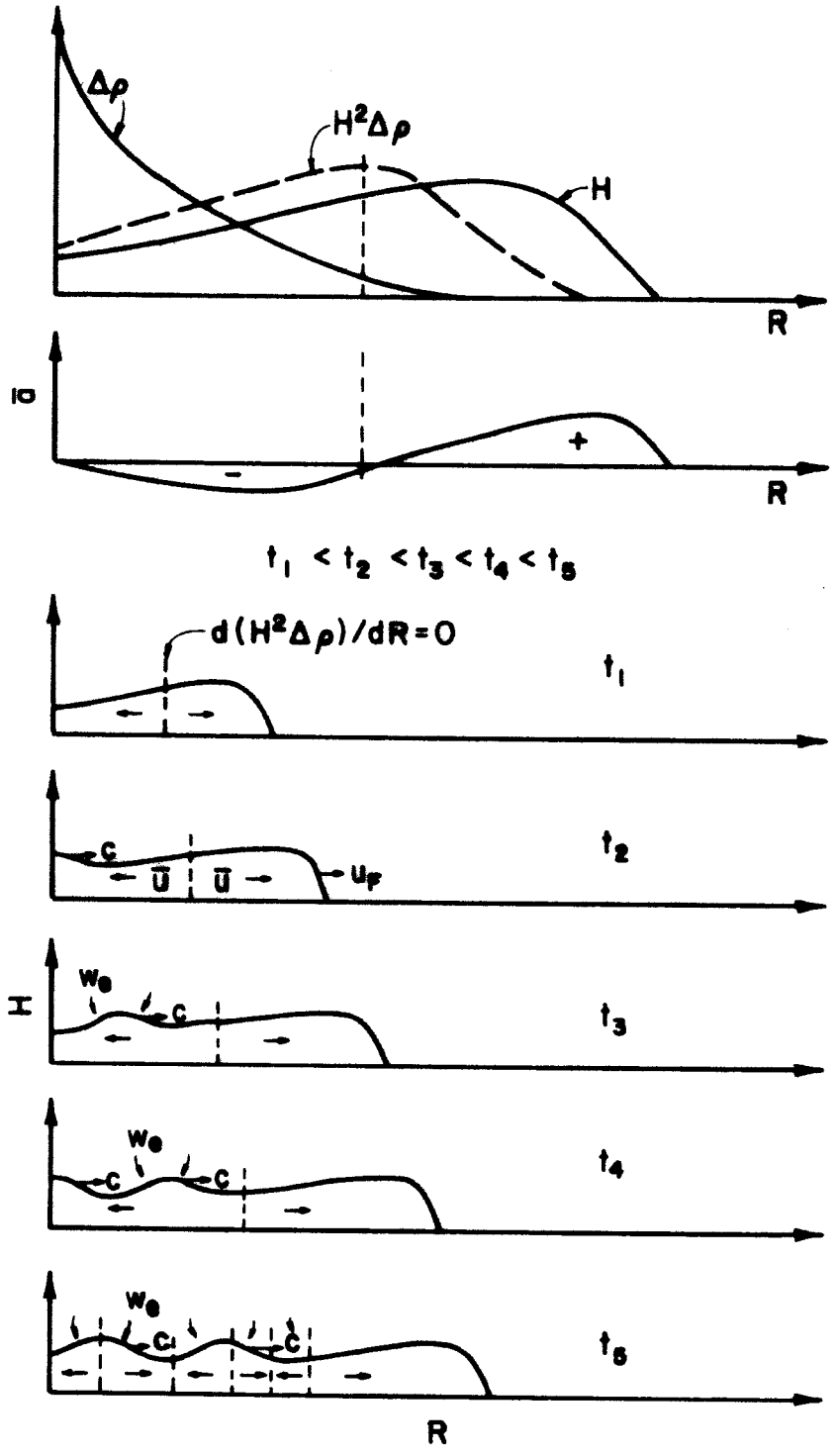

Figure 17. Physics of Surface Waves on Dense Clouds

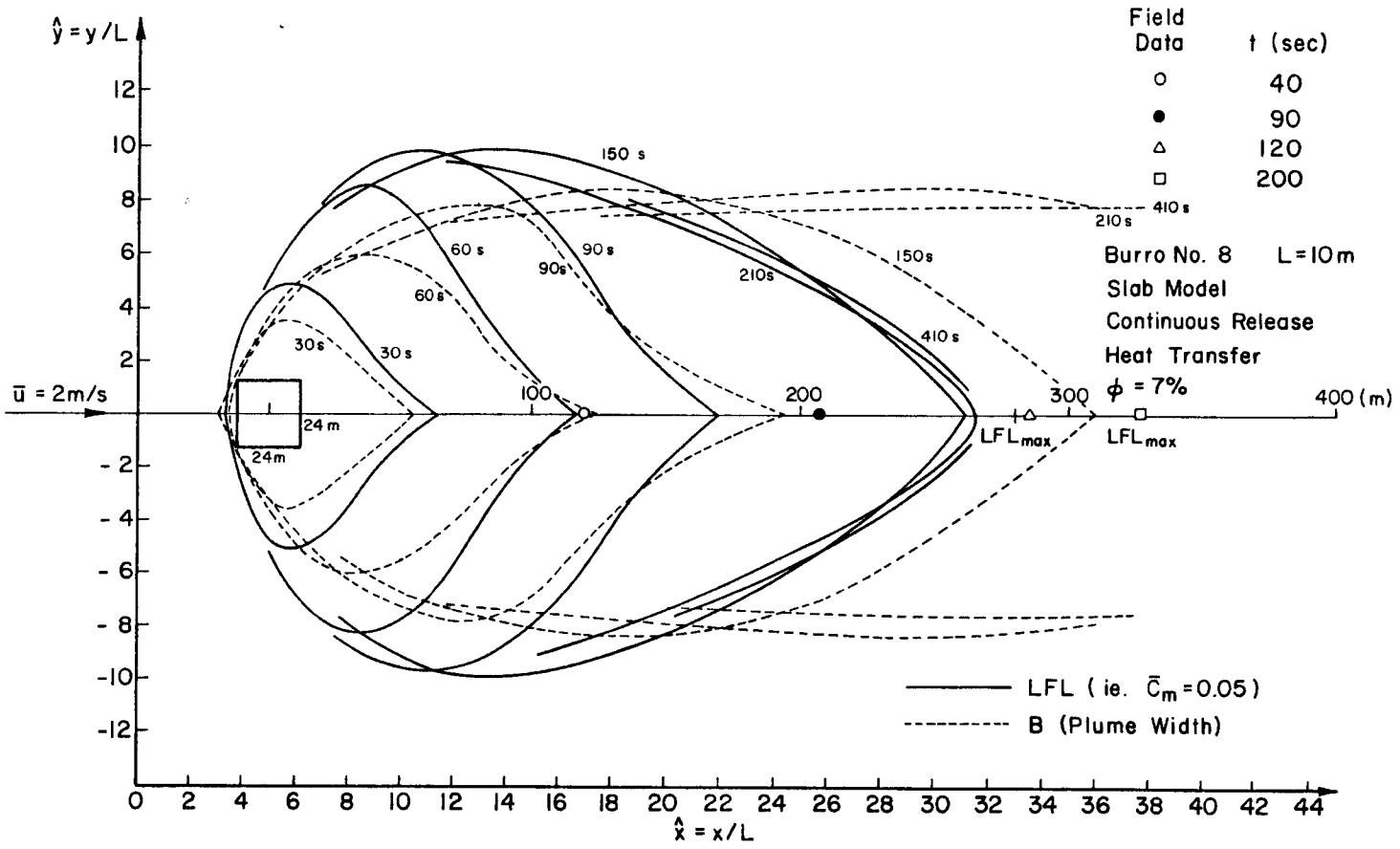

Figure 18. Burro Trial No. 8 - Transient Behavior of the LFL Mean Concentration of 5%, Continuous Boiloff